Bioorganic Chemistry 88 (2019) 102935

Contents lists available at ScienceDirect

Bioorganic Chemistry

journal homepage: www.elsevier.com/locate/bioorg

α-bisabolol β-D-fucopyranoside as a potential modulator of β-amyloid peptide induced neurotoxicity: An *in vitro* & *in silico* study

Mahalingam Jeyakumar[a], Sethuraman Sathya[a], Soniya Gandhi[b], Prabhakarrao Tharra[b], Venkatesan Suryanarayanan[c], Sanjeev Kumar Singh[c], Beeraiah Baire[b], Kasi Pandima Devi[a,*]

[a] Department of Biotechnology, Alagappa University, Karaikudi 630003, Tamil Nadu, India
[b] Department of Chemistry, Indian Institute of Technology Madras, Chennai 600036, Tamil Nadu, India
[c] Computer Aided Drug Design and Molecular Modeling Lab, Department of Bioinformatics, Alagappa University, Karaikudi 630003, Tamil Nadu, India

ARTICLE INFO

Keywords:
α-bisabolol β-D-fucopyranoside (ABFP)
Cholinesterase (ChE)
Oxidative Stress
Amyloid β-protein
Neuroprotective
Alzheimer's disease (AD)

ABSTRACT

Alzheimer's disease (AD) is a multifaceted neurodegenerative disorder affecting the elderly people. For the AD treatment, there is inefficiency in the existing medication, as these drugs reduce only the symptoms of the disease. Since multiple pathological proteins are involved in the development of AD, searching for a single molecule targeting multiple AD proteins will be a new strategy for the management of AD. In view of this, the present study was designed to synthesize and evaluate the multifunctional neuroprotective ability of the sesquiterpene glycoside α-bisabolol β-D-fucopyranoside (ABFP) against multiple targets like acetylcholinesterase, oxidative stress and β-amyloid peptide aggregation induced cytotoxicity. *In silico* computational docking and simulation studies of ABFP with acetylcholinesterase (AChE) showed that it can interact with Asp74 and Thr75 residues of the enzyme. The *in vitro* studies showed that the compound possess significant ability to inhibit the AChE enzyme apart from exhibiting antioxidant, anti-aggregation and disaggregation properties. In addition, molecular dynamics simulation studies proved that the interacting residue between Aβ peptide and ABFP was found to be involved in Leu34 and Ile31. Furthermore, the compound was able to protect the Neuro2 a cells against $A\beta_{25\text{-}35}$ peptide induced toxicity. Overall, the present study evidently proved ABFP as a neuroprotective agent, which might act as a multi-target compound for the treatment of Alzheimer's disease.

1. Introduction

Alzheimer's disease is a progressive neurodegenerative disease associated with memory loss and cognitive deficits in aged people. Worldwide, it is estimated that 36 million people presently suffer from dementia and this number is expected to sharply increase to 114 million by 2050 [1]. AD is characterized by various pathological features like accumulation of extracellular β-amyloid protein and intracellular neurofibrillary tangles. The major therapeutic strategy for the treatment of AD focuses on the restoration of cholinergic functionality to enhance neurotransmission by increasing the acetylcholine availability in the synaptic cleft [2]. In addition, free radicals are inevitably produced by reactive oxygen species (ROS) and oxidative stress, which leads to the damage of the macromolecules such as DNA, protein, and lipids which plays a pivotal role in the onset of AD [3].

Currently, no treatment is available to reverse or stop the progression of the AD. The available AD drug management is based mainly on cholinesterase inhibitors (ChEIs). For example, tacrine, donepezil, galantamine and rivastigmine, which have been approved for clinical use can only modulate the symptoms of AD for a short period of time, or aim at a single target [4] Because of the flexible and complicated etiology, the "one-molecule, one-target" therapy appears not so efficient in treating multifarious diseases like AD. They offer only symptomatic treatment but cannot alleviate the clinical manifestation or development of the disease. Furthermore, many researchers have devoted their efforts for the development of multi-targeted direct ligands (MTDLs), which are single molecules (for example, 4-hydroxyl aurone derivatives and fused tricyclic coumarin derivatives) that can exhibit multiple pharmacological effects, as a positive approach to fight against the multifactorial nature of AD [3,5]. Since the development of

Abbreviations: AD, Alzheimer's disease; Aβ, amyloid β-protein; ABFP, α-bisabolol β-D-fucopyranoside; AChE, acetylcholinesterase; BBB, blood-brain-barrier; DPPH, 1,1-diphenyl-2-picrylhydrazyl; ThT, Thioflavin-T; CLSM, confocal laser scanning microscope; TLC, thin layer chromatography; DMPD, N,N-dimethyl-p-phenylenediamine; MTT, 3-[4,5-dimethyltiazol-2-yl]-2,5-diphenyltetrazolium bromide; DCFH-DA, dichloro-dihydro-fluorescein diacetate

* Corresponding author.
E-mail address: pdevik@alagappauniversity.ac.in (K. Pandima Devi).

https://doi.org/10.1016/j.bioorg.2019.102935
Received 1 March 2019; Received in revised form 8 April 2019; Accepted 15 April 2019
Available online 19 April 2019
0045-2068/

effective MTDLs can act as a promising drug for the treatment of complex diseases such as AD, there is an urgent need to screen for drugs with multiple targets.

Nowadays, efficient compounds are derived from natural products and their derivatives hold several biological properties [6,7]. α-bisabolol is one such natural sesquiterpene alcohol, which is present widely in natural sources such as essential oils of *Matricaria chamomilla* with many medicinal properties. Previous work from our lab has shown that the anti-cholinesterase and anti-aggregation potentials of the marine seaweed *Padina gymnospora* is attributed to the presence of the compound α-bisabolol [8]. However, the major drawback of using α-bisabolol is its insolubility in biological fluids. In order to overcome the short comings of α-bisabolol, the present study aims for synthesis of the α-bisabolol derivative, α-bisabolol β-D-fucopyranoside (ABFP), a glycosidation product of α-bisabolol (which is not commercially available). Moreover, it is a glycosidic sugar compound and it has been reported that the glycosidation of a molecule increases its hydrophilicity, and thereby influencing its physicochemical and pharmacokinetic properties [9]. According to the *in silico* ADME predictions, the glycosidic nature of ABFP has been previously estimated to cross the (blood brain barrier) BBB due to its suitable pharmacokinetics properties like Polar surface area (PSA), Calculated partition coefficient (*clogP)*, and Hydrogen bond donor (HBD) [10]. It is quite conflicting with the purpose of the addition of a glycosides be able to improve BBB porous capacity, whereas Egleton et al. (2001) has shown that the BBB penetrability of a peptide was enhanced by the addition of a glucose molecule [11]. ABFP previously identified from the aerial parts of *Carthamus lanatus* exhibited cytotoxic activity which was evident by the *Artemia salina* assay [12]. In addition, this compound has been evaluated for cytotoxicity against human and rat glioma cancerous cell lines such as (U-87, U-251, and GL-261) cells [10], while the neuroprotective efficacy of the compound is not yet known. Hence an approach has been framed to synthesise the derivative α-bisabolol β-D-fucopyranoside and explore its neuroprotective potential against Alzheimer's disease through *in vitro* and *in silico* systems.

2. Results and discussion

2.1. Synthesis of α-bisabolol β-D-fucopyranoside (ABFP)

To prepare the target ABFP **1**, the glycosyl trichloroacetimidate (TCA) based Schmidt strategy [13,14] was adopted. We coupled the α-bisabolol and α-D-fucopyranosyl trichloroacetimidate **2** to achieve the final product **1**. To begin with, our aim was to synthesize D-fucose based TCA derivative **2** (Scheme 1). Accordingly, D-fucose was treated with benzoyl chloride, pyridine and 10 mol% of 4-dimethylaminopyridine (DMAP), in dichloromethane at RT for 16 h. The corresponding tetrabenzoyl fucose derivative **3** was obtained in 95% yield after chromatographic purification. To do a regio-selective benzoyl deprotection at anomeric position in compound **3**, we chose a two step protocol. Initially, a dichloromethane solution of **3** was treated with HBr (33% in AcOH) at RT for 2.5 h. After washing the reaction mixture with aq. sodium bicarbonate, the crude material was used for next reaction. Treatment of the crude reaction mixture with silver carbonate (Ag_2CO_3) in acetone and water (20:1), at RT for 1.5 h, provided the hydroxylated compound **4** with 80% yield for two mixture of diastereomer (1:0.5). Next, using the Schmidt's procedure, TCA derivative **2** was prepared. Reaction of monohydroxy-compound **4** with tricholoroacetonitrile (CCl_3CN) in presence of cesium carbonate (Cs_2CO_3) at 0 °C for 16 h in CH_2Cl_2 resulted in the formation of fucose-TCA derivative **2** in 70% yield.

Subsequently, with the essential TCA derivative **2** in hand, we focused on the generation of our target molecule α-bisabolol β-D-fucopyranoside **1** (Scheme 2). The α-bisabolol was treated with 10 mol% of TMSOTf in anhydrous CH_2Cl_2 at −78 °C for 15 min. Next, after the addition of an ice cold solution of TCA derivative **2** in DCM was added dropwise to reaction mixture and the reaction was allowed to keep at −20 °C for 2.5 h, after quenching this reaction with triethylamine (Et_3N), reaction afforded the product **5** in 80% yield. Further, the solution of coupled product **5** in H_2O/THF/MeOH (1:2:1 ratio) upon subjection to aq. NaOH (0.25 *N*) for 1.5 h, resulted in the formation of the α-bisabolol β-D-fucopyranoside **1** excellent yield (98%).

2.2. In silico evaluation of ABFP against AChE and β-secretase

2.2.1. Docking analysis of ABFP with AChE & β-secretase

The 3D structure of ABFP were docked with prepared AChE using Glide XP module implemented in Schrödinger. The docking scores were obtained with −9.488 kcal/mol, glide emodel of −31.604 kcal/mol and glide energy of −42.255. The interactions obtained during the docking were evident with the pictorial representation of 2D and 3D interaction of AChE complexed with ABFP represented in (Fig. 1A). It reveals that Asp74 and Thr75 were interacting with ligand through hydrogen bond interaction. Subsequently, the complex were further evaluated for the binding free energy calculation which exhibited the ΔG_{bind} value of −51.810 kcal/mol and found to be supportive for the docking results (Table1).

2.2.2. Molecular dynamics simulation studies with AChE

The complex was further analyzed for molecular dynamics simulation for 20000 ps time period of simulation in order to access the binding interaction stability. The conformational changes in the structure was analyzed through the calculation of root mean square deviation (RMSD) and root mean square fluctuations (RMSF) over backbone atoms. (Fig. 1B) (A) shows that the complex have stable deviations around 1.8 Å after 14000 ps time period of simulation. (Fig. 1B) (B) shows the RMSF of residues of AChE where it reveals that residues from 250 to 270 and 480–500 were fluctuating to the highest of 4.4 Å because they are in loop region. (Fig. 1B) (C) shows the radius of gyration of the protein which clearly shows that the protein does not lose its compactness during the simulation time period. The histogram and the timeline of the protein ligand contacts were represented in (Fig. 1C) which reveals that Tyr72, Thr75, Trp286 and Tyr341 were the most interacting residues over the course period of simulation. During Glide XP docking Asp74 was interacting whereas the same interaction was lost and this is very clearly evident with the (Fig. 1D). It also shows that there is no much changes in the secondary structure of protein during the course period of simulation for 20 ns. MD simulation analysis shows that hydrophobic interaction plays a major role in stabilizing the ligand in its active site whereas the hydrogen bond interaction with Tyr72, Thr75 and Tyr341 plays less important role.

2.3. In vitro evaluation of acetylcholine esterase (AChE) inhibitory activity of ABFP

Acetylcholinesterase is the enzyme present in nervous tissue that helps to break down the neurotransmitter acetylcholine. According to the cholinergic hypothesis, a decrease in the level of acetylcholine in the brain is primarily involved in memory destruction during AD. Since the inhibition of cholinesterase has a significant role for the treatment of AD [15], the present study involved the evaluation of AChE inhibitory potential of ABFP. The results clearly illustrated that, the higher concentration of ABFP (50 μg/ml) showed potent ChE inhibitory activity of 95.869 ± 0.121% when compared with standard drug donepezil whose % of inhibition was 95.856 ± 0.847 (Fig. 2). Several scientific reports illustrate that naturally derived compounds act as a source of new biofunctional scaffolds targeting cholinesterase and β amyloid aggregation [16]. The results of our study suggest that ABFP could be used for anti-cholinergic remedy for AD treatment.

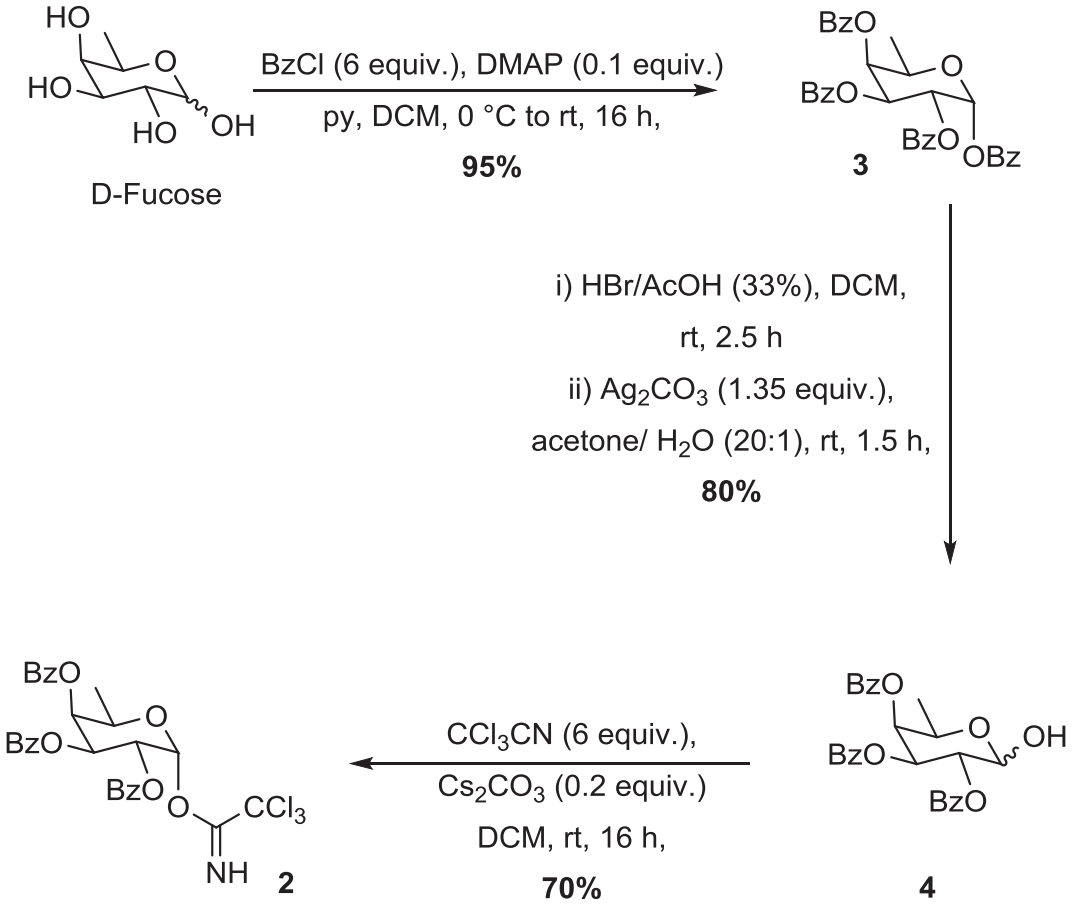

Scheme 1. Preparation of TCA derivative of fucose **2.**

2.4. *In vitro evaluation of antioxidant property of ABFP*

2.4.1. *DPPH radical scavenging activity of ABFP*

DPPH is a free radical that is mostly used for antioxidant studies. Several studies have reported that dysfunction of the neuronal junction is combined with oxidative stress that can involve vital role in AD [17].

The effect of free radical scavenging activity of ABFP was assessed by the DPPH assay. As seen in (Fig. 3A), ABFP exhibited potent radical scavenging activity of 68.9 ± 0.44% at 50 µg/ml when compared with the standard BHT (80.3 ± 1.5%) at 50 µg/ml. The result indicates that high antioxidant potency of the ABFP might be due to its electron or hydrogen donating ability.

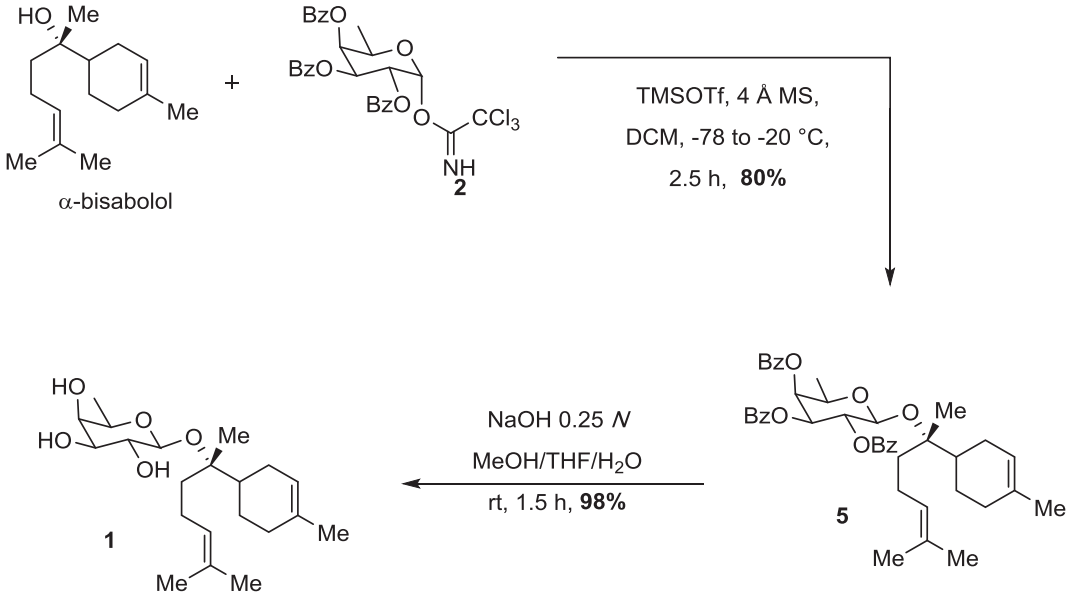

Scheme 2. Synthesis of α-bisabolol β-D-fucopyranoside **1.**

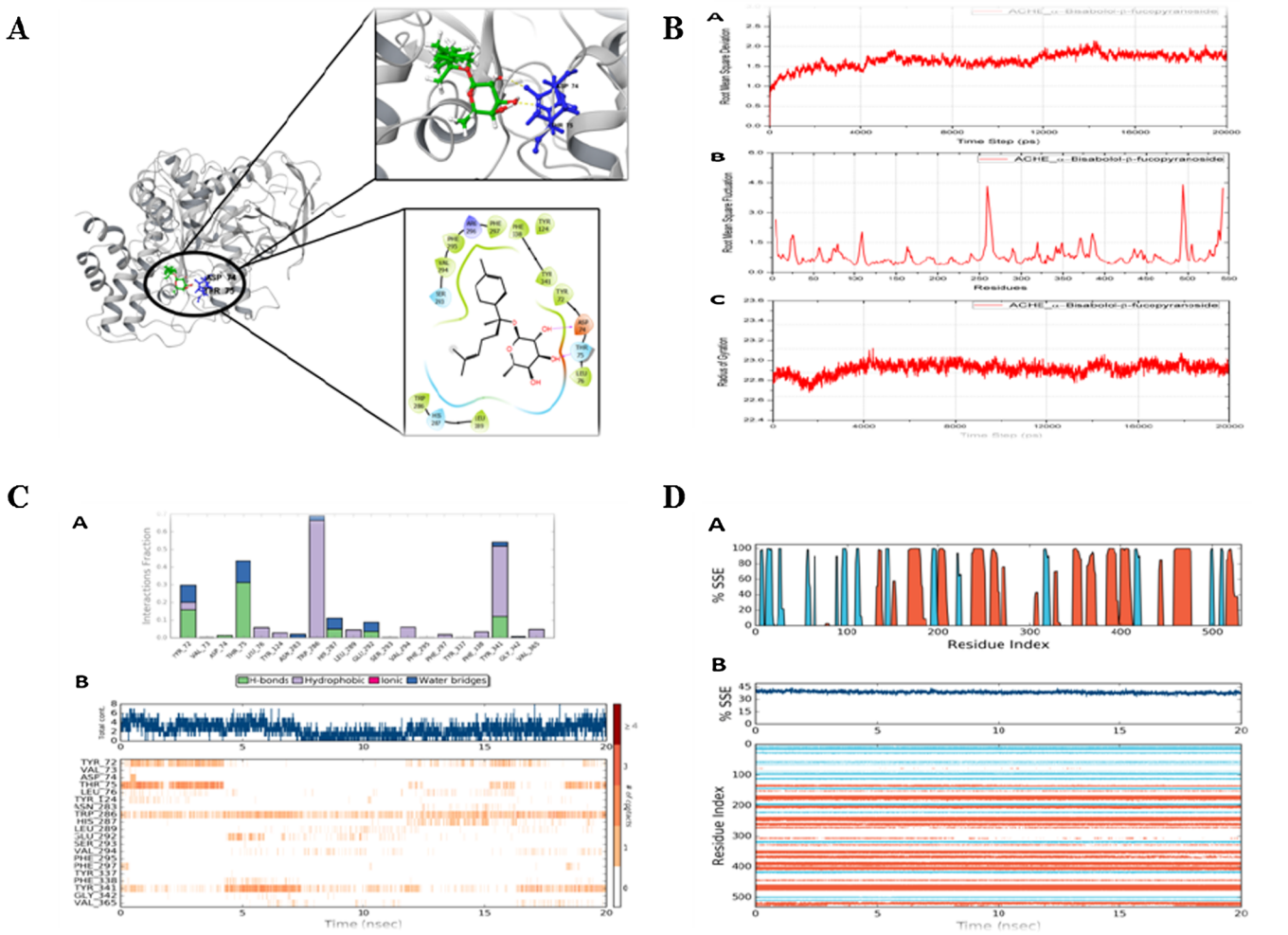

Fig. 1. (A) Result of Glide XP docking representing both three dimensional and two dimensional interaction of ABFP with AChE. **Fig. (B)** RMSD (A), RMSF (B) and Radius of gyration (C) of AChE complexed withABFPover 20000 ps time period of simulation. **Fig. (C)** Histogram (A) and Time line (B) of Protein ligand contact of AChE complexed withABFPover 20000 ps time period of simulation. **Fig. (D)** Histogram and Time line of Secondary Structure Elements (SSE) of AChE complexed with ABFP over 20000 ps time period of simulation.

Table 1
Molecular docking studies with AChE and β-secretase enzymes.

S. no	Protein	Compound	Docking score	Glide Emodel	Glide energy
1	**AChE**	α-bisabolol	−8.482	−26.826	−34.895
2		9-hydroxybisabolol oxide	−6.228	−30.078	−37.019
3		Seco -bisabolol oxide B	−7.142	−33.362	−43.381
4		α-bisabolol β-D-fucopyranoside	−9.488	−31.604	−42.255
5	**β-secretase**	α-bisabolol	−5.095	−31.128	−26.863
6		9-hydroxy bisabolol oxide	−5.096	−27.132	−26.393
7		Seco -bisabolol oxide B	−6.082	−51.272	−39.315
8		α-bisabolol β-D-fucopyranoside	−7.844	−33.600	−40.826

2.4.2. Hydrogen peroxide scavenging potential of ABFP

In living cells, the non reactive hydrogen peroxide when converted into the free radical called as hydroxyl radicals ($OH^{\cdot}$), reacts with macromolecule and causes tissue damage [18]. Hence removing the cytotoxic agent H_2O_2 is very important for protection of human system. The scavenging ability of ABFP on H_2O_2 in comparison with standard L-Ascorbic acid is shown in Fig. 3B. The results exhibited that ABFP showed maximum H_2O_2 scavenging potential of 68.4 ± 0.44% (at 50 µg/ml) when compared with the standard L-ascorbic acid 66.8 ± 0.17% (50 µg/ml). A statistically significant correlation was found between ABFP, standard and control ($P < 0.05$). The data suggests that ABFP possess significant antioxidant activity, which might donate electrons to H_2O_2, thus neutralizing it to water.

2.4.3. Hydroxyl radical scavenging activity of ABFP

Hydroxyl radical is an extremely reactive free radical formed in biological systems and has the capacity to cause DNA strand breakage, which contributes to carcinogenesis, mutagenesis and cytotoxicity [19]. The effect of ABFP on the inhibition of free radical mediated damage was assessed by means of the Fe^{2+} dependent DNA damage assay. The Fenton reaction generates $OH^{\cdot}$, which degrades DNA deoxyribose, using Fe^{2+} salts as catalyst. The hydroxyl radical may attack DNA either at sugar or base giving rise to toxic product. Fig. 3C shows the effect of ABFP on the Fe^{2+} dependent deoxyribose damage. Whereas,

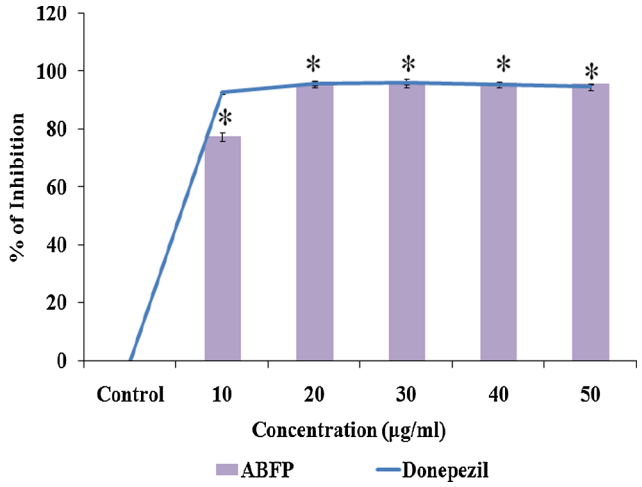

Fig. 2. Acetylcholinesterase inhibitory activity of ABFP in comparison with standard donepezil. (*) denotes significant ($P < 0.05$) inhibitory activity when compared to control. Results are expressed as Mean ± S.D of three parallel measurements.

the higher concentration of ABFP and BHT (50 µg/ml) exhibited strong hydroxyl radical scavenging activity of 73.8 ± 0.22% and 71.7 ± 1.5% respectively. The result anticipated that ABFP has high antioxidant potency against peroxidation of lipids on biological systems through scavenging of hydroxyl radical scavenging activity.

2.4.4. Reducing power of ABFP

Reducing power assay which evaluates the conversion of Fe^{3+} into Fe^{2+} in the presence of ABFP, was measured to determine its reducing power ability. The reducing capability of a compound is a significant marker of its possible antioxidant activity, which generally depends on its ability to donate a hydrogen atom that can reduce the lipid peroxidation process [20]. Fig. 4A shows that ABFP exhibited higher reducing power potential when compared to control and standard L-ascorbic acid. The results of antioxidant assays indicate that ABFP possess greater reducing potential and it can be able to prevent the oxidative stress to cellular components.

2.4.5. Assessment of metal chelating potential of ABFP

The biochemical and neuropathological evidences have suggested that dyshomeostasis of cerebral biometals such as copper, cadmium, zinc, play a major role in Aβ aggregation and neurotoxoticity, which plays a central role in AD pathogenesis. For example, Aβ interaction with metal ions like Cu (II) and Zn (II) and their binding can also induce the toxic peptide aggregation [21]. The results of the present study (Fig. 4B) demonstrated that the formation of ferrozine-Fe^{2+} complex in metal chelating activity is inhibited by ABFP (50 µg/ml), which showed the highest metal chelating activity of 6.25 ± 0.58 when compared to standard BHT 5.15 ± 0.21 (50 µg/ml). Currently, several lipophilic

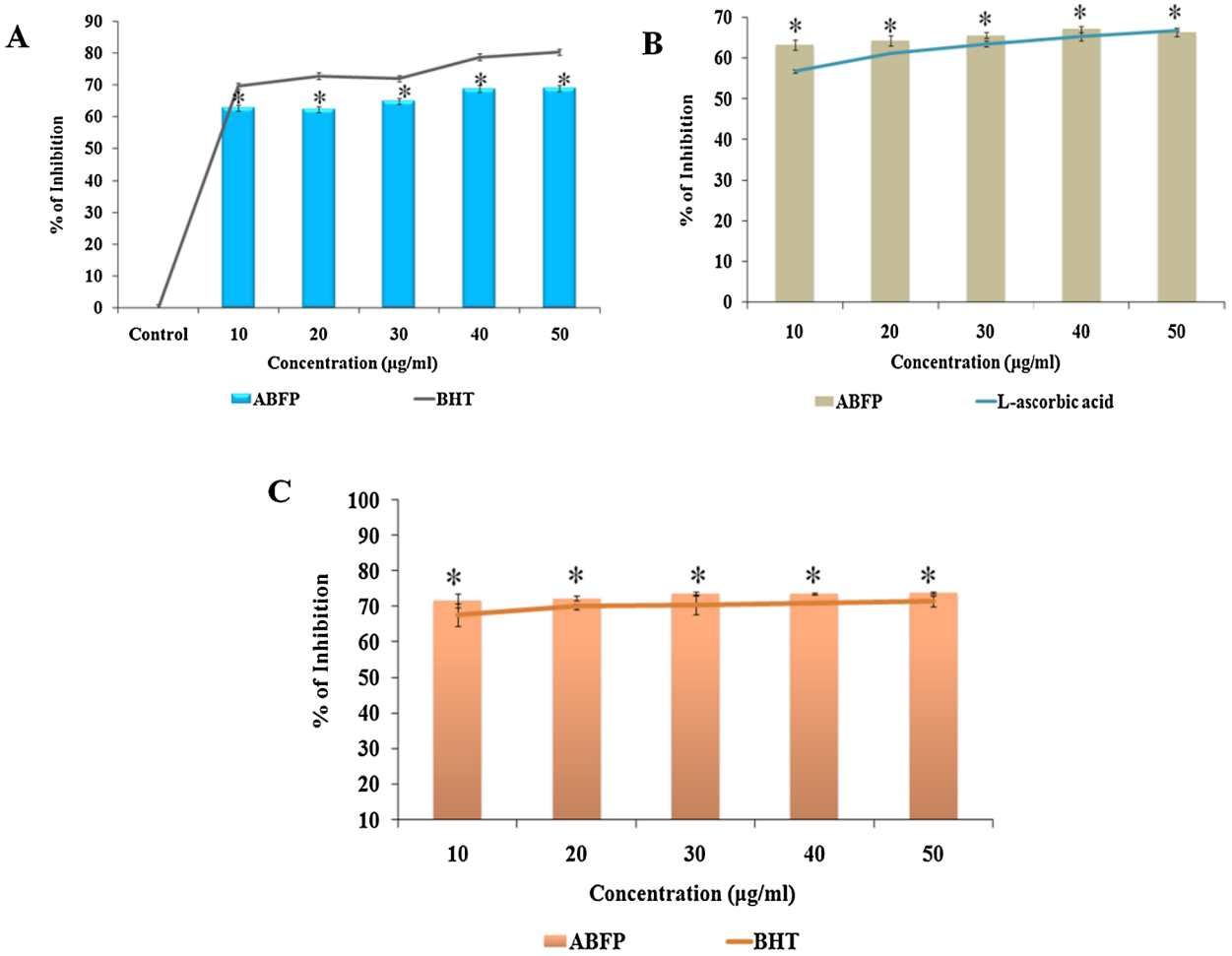

Fig. 3. (A) DPPH free radical scavenging activity of ABFP and BHT. **Fig. (B)** Hydrogen peroxide inhibitory activity of ABFP and standard L- ascorbic acid. **Fig. (C)** Hydroxyl radical scavenging activity of ABFP and BHT. Data were expressed as Mean and S.D (±) of three parallel measurements. (*) Asterisk denotes significant level at ($P < 0.05$) on comparison of drug and control.

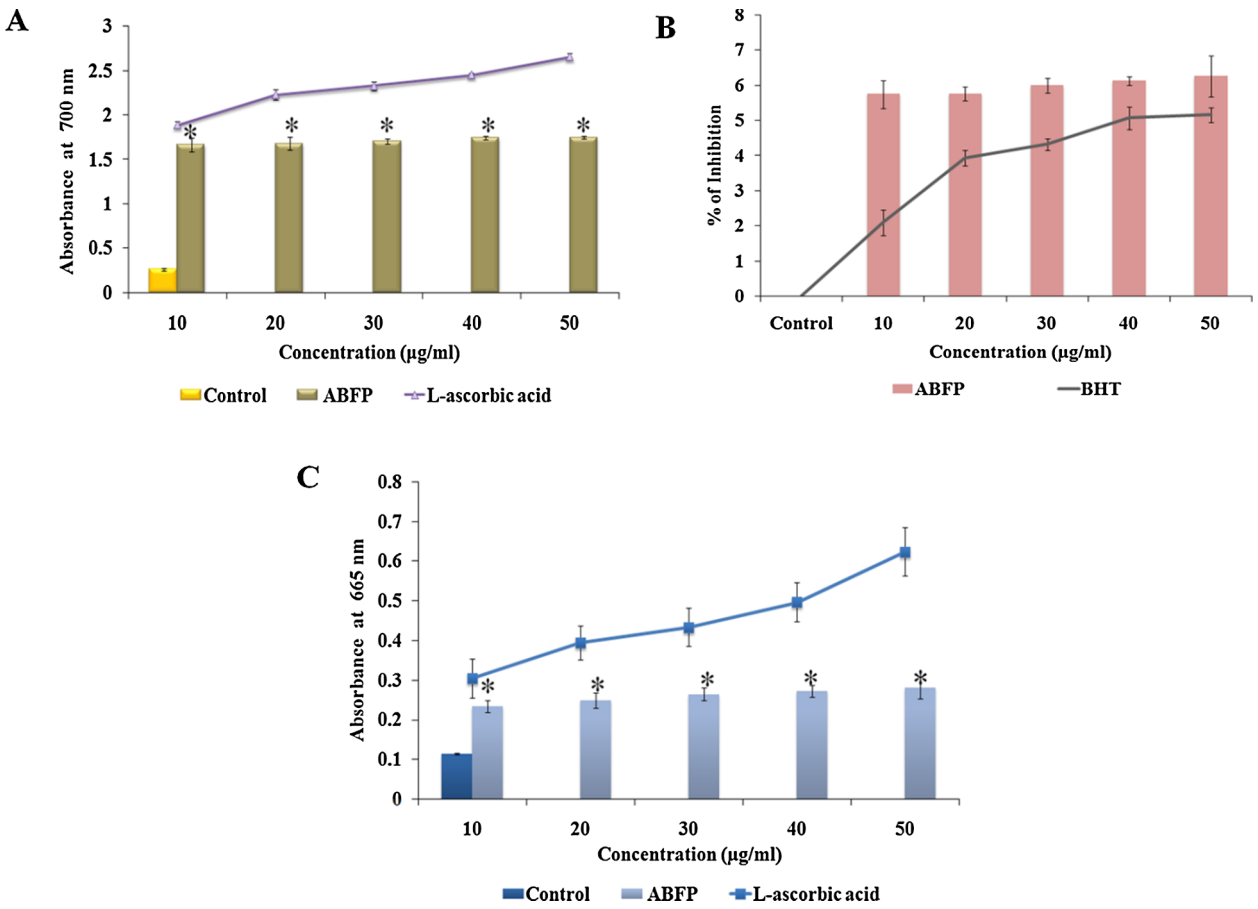

Fig. 4. (A) Reducing power capacity of ABFP in comparison with L- ascorbic acid. **Fig. (B)** Metal chelating activity of ABFP and BHT. **Fig. (C)** Total antioxidant capacity (TAC) of ABFP in comparison with standard L-Ascorbic acid. Asterisk (*) denotes significant ($P < 0.05$) difference between ABFP and control. Each experimental values were calculated as Mean ± Standard deviation (n = 3).

metal chelators for example, clioquinol and its derivative PBT2 have been studied in clinical trials which showed encouraging results in AD patients [22].

2.4.6. Total antioxidant capacity of ABFP

The Total antioxidant capacity (TAC) of ABFP were evaluated by phosphomolybdenum method which shows the ability of a compound to reduction of Mo (VI) to Mo (V) at acidic pH [23]. The results of TAC showed that ABFP exhibited significant *(P < 0.05)* reducing potential with the higher absorbance of 0.281 ± 0.02 at (50 µg/ml) when compared to control 0.114 ± 0.001 and similar to the standard L-ascorbic acid 0.624 ± 0.06 (50 µg/ml) (Fig. 4C) which indicates that it act as an excellent natural antioxidant.

2.5. Effect of ABFP on in vitro aggregation and disaggregation of $A\beta_{25-35}$

2.5.1. Thioflavin T assay

The antiaggregation and disaggregation property of Aβ peptide was quantified by Thioflavin T (ThT) assay [24]. ThT is a fluorescent dye that is used for quantification of Aβ peptide. This assay was performed at different time interval (24 h, 48 h, 96 h and 9d) in two different phases, namely, phase I & phase II (Fig. 5A).

Phase I: Inhibition of formation of aggregates from oligomers: In phase I study, Thioflavin – T fluorescence intensity was found to increase in Aβ peptide group from 24 h (21.49 ± 2.41 AU) to 48 h (27.61 ± 1.44) which indicated the commencement of Aβ peptide aggregation. However, upon treatment with ABFP (5 & 10 µg/ml), reduction in the (ThT) fluorescence was observed at 24 h (17.43 ± 2.84 AU, 13.5 ± 0.86 AU respectively) and 48 h (6.65 ± 1.97 AU, 6.79 ± 0.76 AU respectively) when compared to the standard drug galantamine (50 µg/ml) (11.81 ± 2.84 AU at 24 h & 6.00 ± 1.97 AU at 48 h). Thus the result of phase I study indicated the capability of ABFP to inhibit oligomer formation and thereby confirms its anti-aggregation property (Fig. 5B).

Phase II: Disaggregation of the pre-formed mature fibrils: The results of phase II study showed that an increase in (ThT) fluorescence intensity was observed from 96 h (29.97 ± 1.40 AU) to 9 days (35.18 ± 2.00 AU). However, reduced ThT fluorescence intensity treatment wwas observed during ABFP (5 & 10 µg/ml) and galantamine in 96 h (14.4 ± 1.02 AU, 3.84 ± 1.2 AU) & (6.54 ± 1.02 AU) and 9 days (14.46 ± 1.89 AU, 7.30 ± 1.79 AU) & (15.14 ± 1.16 AU) treatment. The results clearly indicated that ABFP might disaggregate the mature fibrils (Fig. 5B). Therefore, the result highlighted the potential of ABFP to inhibit Aβ aggregation and disaggregation in both phase I & II. This data provides a novel hint that ABFP may be used as an anti-amyloidogenic lead for AD.

2.5.2. Microfluorescence assay

The results were additionally confirmed by CLSM analysis. The confocal image confirmed that less peptide aggregation were observed at 24 h & 48 h, whereas the peptide aggregation was enhanced at 96 h & 9 d in $A\beta_{25-35}$ treated group. Co-treatment with ABFP (5 & 10 µg/ml) exhibited anti-aggregation and dis-aggregation property, which was similar as galantamine treated group (Fig. 5C). Hence the data revealed that ABFP and galantamine effectively caused anti-aggregation and also disaggregated the pre-formed mature fibrils of $A\beta_{25-35}$ during the incubation period of 24 h to 9 days, when compared to control.

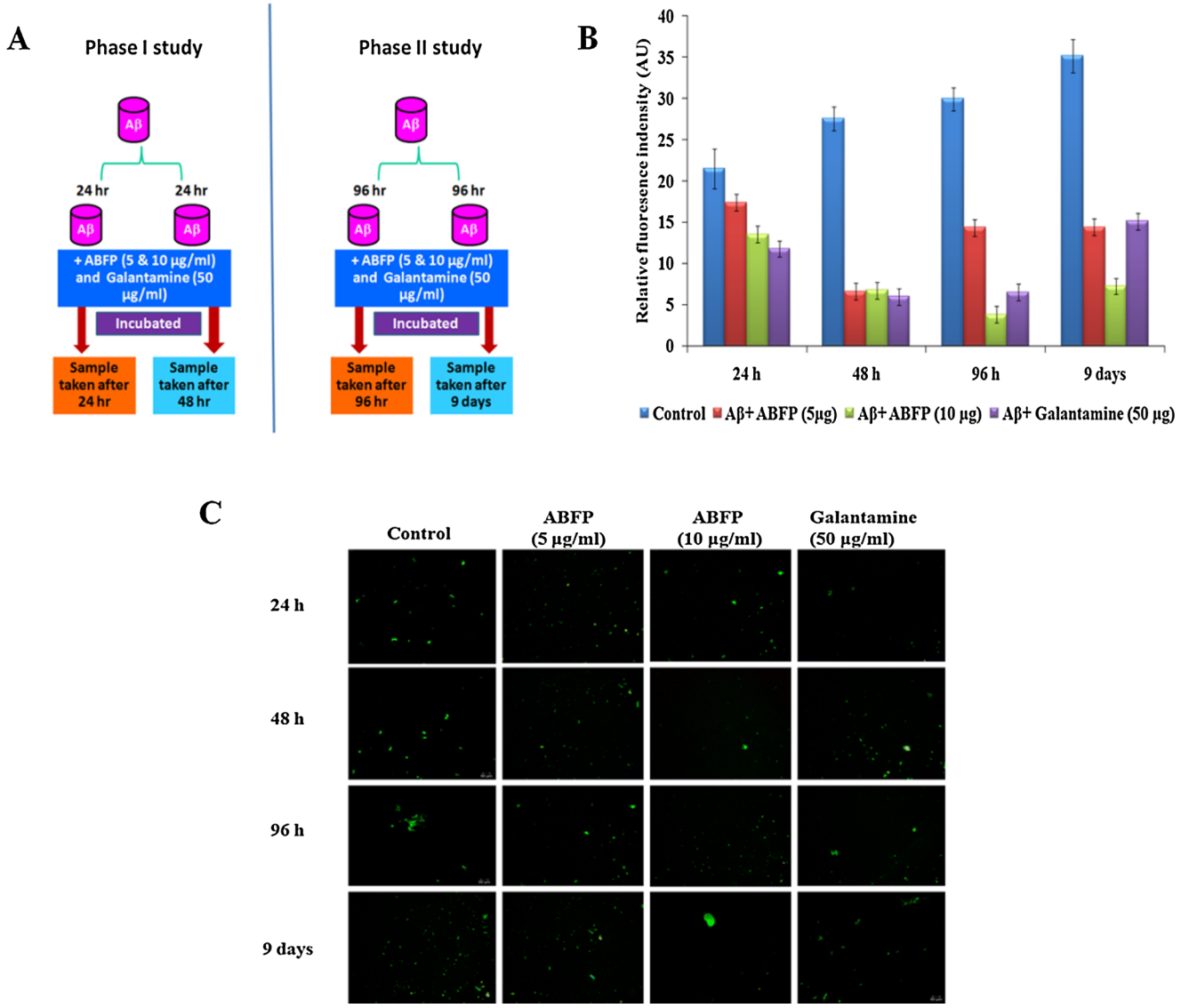

Fig. 5. (A) Design for phase I (24 h & 48 h) & phase II (96 h & 9 days) study. **Fig. (B)** Effect of anti-aggregation and disaggregation pattern of Aβ peptide in various time intervals (24 h and 48 h & 96 h and 9 d respectively) in the presence of ABFP (5 & 10 µg/ml) and Galantamine (50 µg/ml). **Fig. (C)** Confocal Laser Scanning Microscopic image of Aβ peptide alone, ABFP (5 & 10 µg/ml) and Galantamine (50 µg/ml).

2.5.3. Molecular dynamics simulation studies with $A\beta_{25-35}$

The molecular dynamics simulation of the Aβ peptide was performed in order to achieve better understanding of peptide aggregation and the role of ABFP in inhibition of Aβ aggregation for a period of 100 ns simulation. The conformational changes and the aggregation of Aβ peptides were monitored throughout the period of simulation. During simulation, it was observed that ABFP plays a noteworthy role in inhibition of Aβ peptide aggregation which is evident from Fig. 6A. It was observed from the figure that formation of β-sheets has not been noted throughout the simulation time period due to the presence of ABFP which confirmed the anti-aggregation property. Fig. 6B shows the interacting residues between Aβ peptide and ABFP in which Leu34 of Peptide 2 and Ile31 of Peptide 5 was found to be involved in interaction.

2.6. In vitro cell survival of ABFP in Neuro2a cells

MTT assay [25] was performed to evaluate the protective effect of ABFP (2.5–10 µg/ml) in Neuro2a cells. The results suggest that ABFP increased the viability of cells in a concentration dependent manner for 24 h. At the concentration of 5 & 10 µg/ml of ABFP, cell viability was observed to be 94.3 ± 0.05% and 95.2 ± 0.05% respectively (Fig. 7A). Hence, this concentration was fixed for further experimental analysis.

2.6.1. Assessment of protective effect of ABFP against $A\beta_{25-35}$ induced toxicity by MTT assay

The neuroprotective efficacy of ABFP against $A\beta_{25-35}$ in Neuro2a cells were evaluated by MTT assay. Treatment of Neuro2a cells with $A\beta_{25-35}$ peptide reduced the cell viability up to 60% when compared to control. Conversely, pre-treatment with ABFP (5 & 10 µg/ml) significantly ($P < 0.05$) increased the viability of cells to 81.2 ± 0.05% and 96.33 ± 0.06% when compared with control (100%) and standard drug donepezil (50 µg/ml) (78.57 ± 0.05%) (Fig. 7B). In addition, these results were further confirmed through phase contrast microscopic examination of the morphology of cells. The phase contrast microscopic image clearly illustrated that loss of cell to cell contact and reduced cell viability was observed in $A\beta_{25-35}$ treatment group, whereas, after treatment with ABFP (5 & 10 µg/ml), neuronal outgrowth between cells and increase in the cell viability was obtained as similar to that the control group (Fig. 7C).

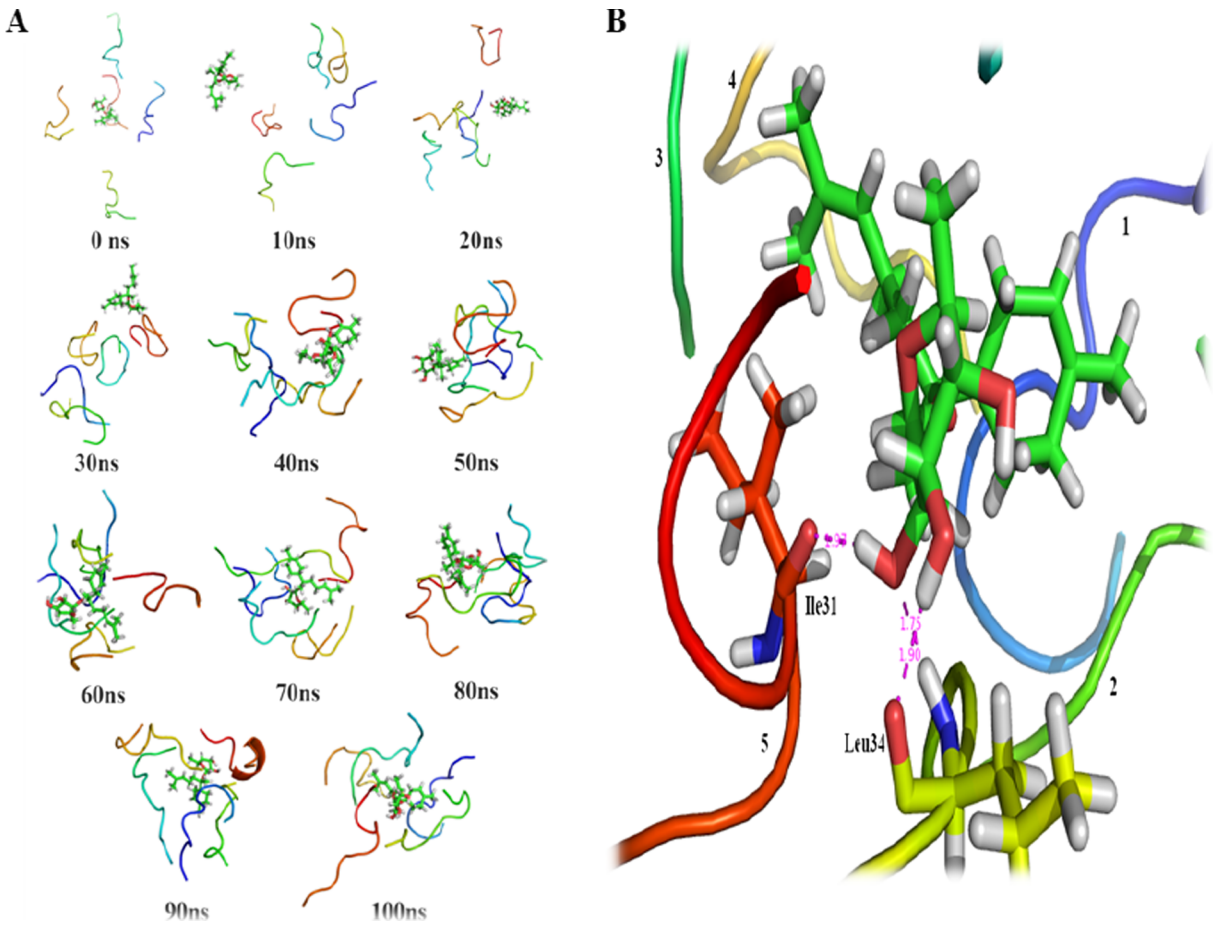

Fig. 6. (A) Position of the randomly placed $A\beta_{25\text{-}35}$ aggregation in the presence of ABFP during 100 ns time period of molecular dynamics simulation at each 10 ns time interval. Interaction of ABFP to $A\beta_{25\text{-}35}$ peptide prevented the formation of β-sheet structure throughout the simulation period. **Fig. (B)** Interaction image of the final structures of five copies of $A\beta_{25\text{-}35}$, which binds with ABFP after 100 ns of molecular dynamics simulation. It binds to Leu34 of Peptide 2 and Ile31 of Peptide 5. These interacting residues were major amino acid residues involved in the oligomerisation. The ligand interfered with the residues and interrupted the aggregate formation.

2.6.2. Effect of ABFP on ROS production in $A\beta_{25\text{-}35}$ treated Neuro2a cells

The production of ROS is considered to be an important pathophysiological event of AD. This may cause deleterious effects to biomolecules like DNA damage, protein and lipid oxidation leading to neuronal dysfunction [26]. In the present study (Fig. 8), treatment of $A\beta_{25\text{-}35}$ (50 μM) with Neuro2a cells for 24 h increased the content of ROS production to about (529.75 ± 3.29 A.U) when compared to the control group (319.09 ± 2.47 A.U). However, pretreatment (for 2 h) with the fixed concentration of ABFP (5 & 10 μg/ml) exhibited significant reduction in the ROS formation (433.31 ± 2.84 & 411.95 ± 3.77 respectively). The results indicate that treatment of Neuro2a cells with ABFP inhibited the ROS production induced by the Aβ peptide.

3. Conclusions

The synthesized compound α-bisabolol β-D-fucopyranoside (ABFP) act as a multipotent agent for the treatment of Alzheimer's disease by impeding the cholinergic neurotransmission, oxidative stress, acting as metal chelators and preventing Aβ aggregation in both *in vitro* and *in silico* experiments. In addition, ABFP exhibited no cytotoxicity and also had neuroprotective effect against $A\beta_{25\text{–}35}$ induced neurotoxicity in Neuro2a cells. Overall, all the experimental results concluded that ABFP act as a promising multi-target agent for the management of AD.

4. Experimental sections

4.1. Chemicals

Acetylcholinesterase (AChE) from Electric eel and Thioflavin T (ThT) were purchased from Sigma Aldrich, USA. Acetylthiocholine iodide (ATCI) and 5,5- Dithio-bis(2-nitrobenzoicacid (DTNB) were obtained from Hi-media Chemicals, Mumbai, India. $A\beta_{25\text{–}35}$ peptide was procured from GenScript USA, Inc. α -bisabolol was acquired from Alfa Aesar Chemical Manufacturing Company, USA. All other reagents, solvents and chemicals used for the experiments were of high grade and purity.

4.2. General procedure for the synthesis of α-bisabolol β-D-fucopyranoside

4.2.1. (2R,3R,4S,5S,6R)-6-Methyltetrahydro-2H-pyran-2,3,4,5-tetrayl tetrabenzoate (3)

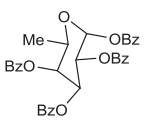

An ice cold solution of α-fucose (500 mg, 3.0 mmol) and DMAP (73 mg. 0.6 mmol) in pyridine (5 mL) and dichloromethane (6 mL), was

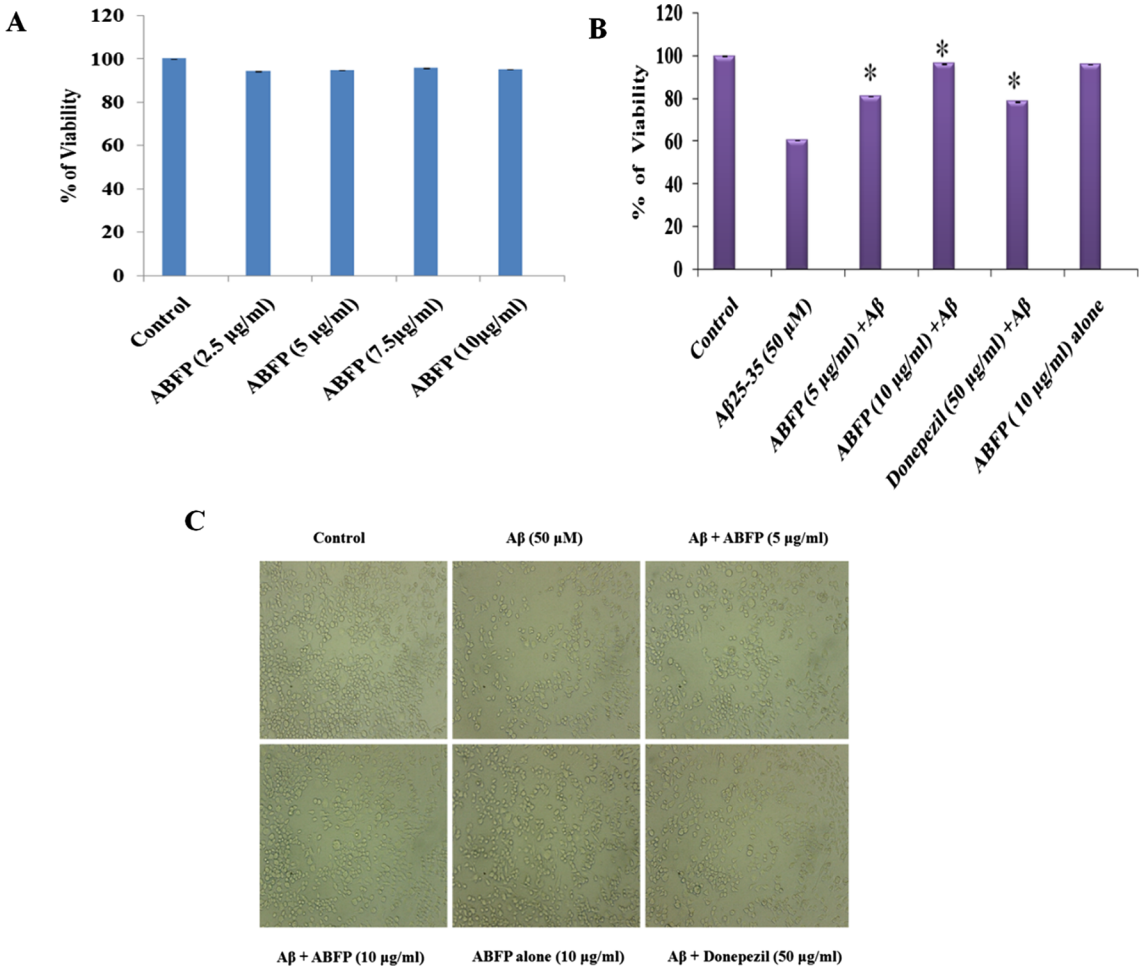

Fig. 7. (A) *In vitro* cytotoxicity of various concentration of ABFP (2.5–10 µg/ml) in Neuro 2a cells for 24 h. **Fig. (B)** The protective effect of ABFP (5 & 10 µg/ml) against $A\beta_{25\text{-}35}$ treatment in Neuro 2a cells **Fig. (C).** Phase contrast microscopic examination of the neuroprotective effect of ABFP and standard drug donepezil against $A\beta_{25\text{-}35}$ neurotoxicity. Values are represented as Mean ± S.D of three parallel measurements. Asterisk (*) denotes ($P < 0.05$) significant difference between $A\beta_{25\text{-}35}$ and ABFP.

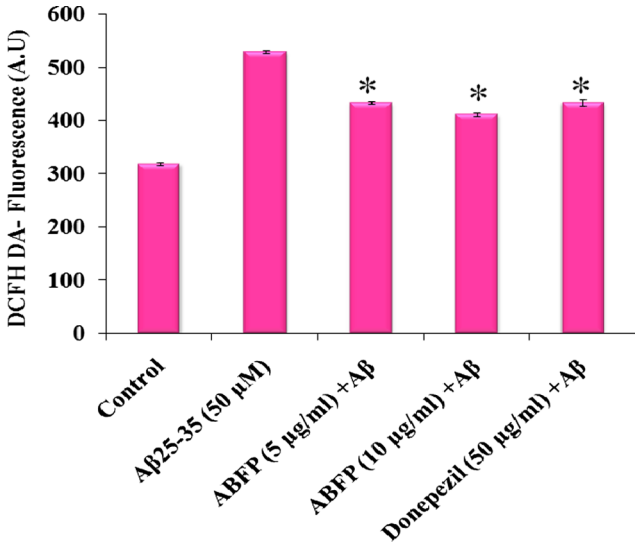

Fig. 8. Effect of ABFP (5 & 10 µg/ml) and $A\beta_{25\text{-}35}$ treatment on ROS formation. Values are represented as Mean ± S.D of three parallel measurements. Asterisk (*) denotes ($P < 0.05$) significant difference between $A\beta_{25\text{-}35}$ and ABFP.

stirred at 0 °C for 15 min. Next the BzCl was added (2 mL, 18.0 mmol) to the reaction mixture slowly and stirring was carried for 16 h. The reaction mixture was diluted by CH_2Cl_2 (20 mL) and 1 *N* H_2SO_4 (15 mL) and washed with $NaHCO_3$ and brine solution. The combined organic layer was dried over $MgSO_4$. Evaportion of the solvent under reduced pressure and purification of the crude by flash column chromatography (Hex/EtOAc, 4:1) gave the benzoyl protected compound **3** as a white foam (1.6 g, 2.7 mmol, 95%).

^{1}H NMR (400 MHz, $CDCl_3$): δ = 8.14–8.11 (m, 4H), 7.87–7.81 (m, 4H), 7.67–7.62 (m, 2H), 7.54–7.58 (m, 4H), 7.47–7.43 (m, 2H), 7.30–7.25 (m, 4H), 6.87 (d, 1H, J = 3.6 Hz), 6.08 (dd, 1H, J = 10.6 & 3.6 Hz), 5.99 (dd, 1H, J = 10.6 & 3.6 Hz), 5.91–5.89 (m, 1H), 4.64 (q, 1H, J = 7.0 Hz) and 1.32 (d, 3H, J = 6.5 Hz) ppm.

^{13}C NMR (100 MHz, $CDCl_3$): δ = 166.1, 165.9, 167.7, 164.8, 138.9, 133.8, 133.7, 133.5, 133.4, 130.3, 130.1, 130.0, 129.9, 129.4, 129.3, 128.9, 128.8, 128.6, 128.5, 128.4, 90.9, 71.5, 69.1, 68.0, 67.8 and 16.4 ppm.

IR (neat): 2816, 1725, 1593, 1382, 1348, 1264, 1173, 1033 and 716 cm^{-1}.

HR ESI-MS: $[C_{34}H_{28}O_9Na]^+ = [M + Na]^+$ Require 603.1626; found 603.1638.

TLC: R_f = 0.4 (4:1 Hex/EtOAc).

4.2.2. (3R,4R,4S,5S,6R)-2-Hydroxy-6-methyltetrahydro-2H-pyran-3,4,5-triyl tribenzoate (4)

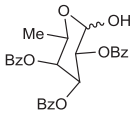

To a solution of the compound **3** (1.6 g, 2.7 mmol) in CH_2Cl_2 (7 mL), HBr was added (1.5 mL, 33% in AcOH) under Ar-atmosphere. The reaction was stirred at RT for 2.5 h. Reaction mixture was quenched with saturated $NaHCO_3$ and extracted with CH_2Cl_2 solvent. The combined organic layer was washed with brine solution, and dried over $MgSO_4$. Solvent was evaporated under reduced pressure. The residue was dissolved in acetone (10 mL), H_2O (0.5 mL) and CH_2Cl_2 (1 mL). The Ag_2CO_3 (1 g, 3 mmol) was added in portions, to the reaction mixture and allowed the reaction to stirr for 1.5 h at RT. The reaction mixture was filtered out through celite and $MgSO_4$. The filtered residue was evaporated under reduced pressure and purified by flash column chromatography (Hex/EtOAc, 7:3) to give α,β isomer, i.e. compound **4** as white foam (1.1 g, 2.0 mmol, 80%).

Diastereomer ratio (1:0.5)

^{1}H NMR (400 MHz, $CDCl_3$): δ = 8.12–8.10 (m, 3H), 7.99–7.95 (m, 3H), 7.81–7.77 (m, 3H), 7.64–7.59 (m, 2H), 7.51–7.47 (m, 4H), 7.44–7.41 (m, 1H), 7.39–7.32 (m, 2H), 7.28–7.21 (m, 3H), 6.04–6.01 (dd, 1H, *J* = 10.5 & 3.3 Hz), 5.78 (d, 1H, *J* = 3.3 Hz), 5.72 (d, 1H, *J* = 2.6 Hz), 5.61–5.57 (m, 1H), 5.01 (d, 1H, *J* = 7.7 Hz), 4.66 (q, 1H, *J* = 6.6 Hz), 4.13 (q, 1H, *J* = 6.2 Hz), 1.36 (d, 3H, *J* = 6.4 Hz) and 1.27 (d, 3H, *J* = 6.4 Hz) ppm.

^{13}C NMR (100 MHz, $CDCl_3$): δ = 166.2, 166.2, 165.8, 133.5, 133.2, 130.1, 130.0, 129.9, 129.8, 129.4, 128.7, 128.6, 128.4, 91.1, 72.2, 69.7, 68.6, 65.2 and 16.3 ppm.

IR (neat): 3402, 2922, 1725, 1593, 1453, 1385, 1105, 1068, 832 and 711 cm^{-1}.

HR ESI-MS: $[C_{27}H_{24}O_8Na]^+$ = [M + Na]$^+$ Require 499.1363; found 499.1370.

TLC: R_f = 0.4 (7:3 Hex/EtOAc).

4.2.3. (2R,3S,4S,5R,6R)-2-Methyl-6-(2,2,2-trichloro-1-iminoethoxy) tetrahydro-2H-pyran-3,4,5-triyl tribenzoate (2)

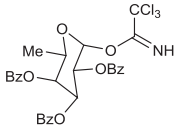

To a solution of the compound **4** (1.1 g, 2.3 mmol) in anhydrous CH_2Cl_2 (7 mL), CCl_3CN (1.2 mL, 11.5 mmol) and Cs_2CO_3 (110 mg, 0.33 mmol) were added. The reaction mixture was stirred for 16 h at RT and filtered out through celite using CH_2Cl_2 solvent. The solvent was evaporated under reduced pressure and the crude mixture was purified by flash chromatography (Hex/EtOAc, 7:3) to give the compound **2** (1 g, 1.46 mmol, 70%) as a white foam.

^{1}H NMR (400 MHz, $CDCl_3$): δ = 8.66 (s, 1H), 8.12–8.10 (m, 2H), 7.96–7.94 (m, 2H), 7.82–7.79 (m, 2H), 7.66–7.61 (m, 1H), 7.53–7.48 (m, 3H), 7.46–7.42 (m, 1H), 7.35 (t, 2H, *J* = 7.6 Hz), 7.26 (t, 2H, *J* = 7.6 Hz), 6.83 (d, 1H, *J* = 3.6 Hz), 6.06–6.02 (m, 1H), 5.93–5.90 (m, 1H), 5.89–5.87 (m, 1H), 4.65 (q, 1H, *J* = 6.4 Hz) and 1.30 (d, 3H, *J* = 6.5 Hz) ppm.

^{13}C NMR (100 MHz, $CDCl_3$): δ = 166.0, 165.8, 165.7, 160.9, 133.7, 133.6, 133.4, 130.1, 129.9, 129.8, 129.3, 129.1, 128.9, 128.8, 128.5, 128.4, 94.3, 71.5, 68.8, 68.2, 68.0 and 16.4 ppm.

HR ESI-MS: $[C_{29}H_{24}Cl_3NO_8Na]^+$ = [M + Na]$^+$ Require 642.0460; found 642.0429.

TLC: R_f = 0.4 (4:1 Hex/EtOAc).

4.2.4. (2R,3S,4S,5R,6S)-2-Methyl-6-{[(2S)-6-methyl-2-(4-methylcyclohex-3-en-1-yl)hept-5-en-2-yl]oxy}tetrahydro-2H-pyran-3,4,5-triyl tribenzoate (5)

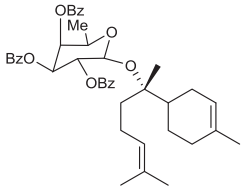

To a solution of α-bisabolol (53 mg, 0.24 mmol) in anhydrous CH_2Cl_2 (3 mL) 4 Å molecular sieves and TMSOTf (5.4 mg, 0.024 mmol) were added at −78 °C under inert atmosphere. An ice cold solution of the compound **2** (300 mg, 0.48 mmol) in anhydrous CH_2Cl_2 was added to the reaction mixture drop wise. Reaction was warmed to −20 °C for 2.5 h. After completion of α-bisabolol, the reaction was quenched by the triethylamine (4 equiv., 100 mg, 0.15 mL, 0.96 mmol). The organic solvent was evaporated under reduced pressure and the crude mixture was purified by flash column chromatography (Hex:EtOAc, 4:1) to give the compound **5** (130 mg, 0.19 mmol, 80%) as a white foam.

^{1}H NMR (500 MHz, $CDCl_3$): δ = 8.20–8.09 (m, 2H), 8.00–7.88 (m, 2H), 7.81–7.73 (m, 2H), 7.65–7.56 (m, 1H), 7.53–7.45 (m, 3H), 7.44–7.31 (m, 3H), 7.27–7.19 (m, 2H), 5.78 (dd, 1H, *J* = 10.5 & 7.8 Hz), 5.69 (d, 1H, *J* = 3.3 Hz), 5.57 (dd, 1H, *J* = 10.5 & 6.8 Hz), 5.18 (broad s, 1H), 5.06 (t, 1H, *J* = 7.0 Hz), 4.92 (d, 1H, *J* = 7.8 Hz), 4.03 (dd, 1H, *J* = 12.9 & 6.5 Hz), 2.32–2.22 (m, 1H), 2.07–1.91 (m, 1H), 1.90–1.84 (m, 1H), 1.84–1.80 (m, 1H), 1.78–1.74 (m, 1H), 1.73–1.70 (m, 1H), 1.67 (s, 3H), 1.64–1.63 (m, 1H), 1.60 (s, 3H), 1.59–1.56 (m, 1H), 1.55 (s, 3H), 1.49–1.42 (m, 1H), 1.30 (d, 3H, *J* = 6.4 Hz), 1.06 (s, 3H) and 0.98–0.86 (m, 1H) ppm.

^{13}C NMR (125 MHz, $CDCl_3$): δ = 166.3, 165.8, 165.3, 134.3, 133.4, 133.2, 133.1, 131.3, 130.2, 129.8, 129.7, 129.5, 129.1, 128.6, 128.4, 128.3, 124.9, 120.2, 95.7, 82.3, 72.5, 71.4, 70.1, 69.6, 40.5, 38.2, 30.8, 29.8, 26.7, 25.8, 23.4, 22.8, 21.7, 19.8, 17.9 and 16.6 ppm.

IR (neat): 2969, 2923, 2856, 1729, 1594, 1450, 1263, 1172, 1101, 1023 and 708 cm^{-1}.

HR ESI-MS: $[C_{42}H_{48}O_8Na]^+$ = [M + Na]$^+$ Require 703.3241; found 703.3210.

TLC: R_f = 0.4 (4:1 Hex/EtOAc).

4.2.5. (2R,3R,4S,5R,6S)-2-Methyl-6-{[(2S)-6-methyl-2-(4-methylcyclohex-3-en-1-yl)hept-5-en-2-yl]oxy}tetrahydro-2H-pyran-3,4,5-triol (1)

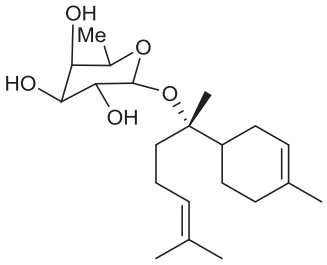

To a solution of the compound **5** (130 g, 0.19 mmol) in MeOH/THF/H_2O (1:2:1; 6 mL), aq. NaOH (2 mL, 0.25 *N*) was added slowly and continued the stirring at RT for 1.5 h. The activated Amberlite (with 1 *N* H_2SO_4) was added to the reaction mixture to pH 7 then reaction mixture was filtered and solvent was evaporated under reduced pressure. Purification of the crude mixture by column chromatography (Hex:EtOAc, 1:1) gave the compound **1** (69 mg, 0.18 mmol, 98%) as a white solid.

^{1}H NMR (400 MHz, $CDCl_3$): δ = 5.35 (broad s, 1H), 5.04 (broad t, 1H, *J* = 6.6 Hz), 4.39(d, 1H, *J* = 6.9 Hz), 3.70 (broad s, 1H), 3.66–3.50

(m, 3H), 2.20–2.10 (m, 1H), 2.0–1.90 (m, 5H), 1.79–1.74 (m, 2H), 1.67 (s, 3H), 1.64 (s, 3H), 1.59 (s, 3H), 1.57–1.53 (m, 1H), 1.52–1.44 (m, 1H), 1.29 (d, 3H, J = 5.8 Hz), 1.24–1.22 (m, 1H) and 1.13 (s, 3H) ppm.

^{13}C NMR (100 MHz, $CDCl_3$): δ = 134.5, 131.2, 124.9, 120.6, 97.1, 81.9, 74.3, 71.9, 71.8, 70.4, 41.0, 37.9, 31.0, 29.8, 26.9, 25.8, 23.5, 21.8, 20.2, 17.9 and 16.6 ppm.

HR ESI-MS: $[C_{21}H_{36}O_5Na]^+$ = **[M + Na]** $^+$ Require 391.2455; found 391.2487

TLC: R_f = 0.4 (1:1 Hex/EtOAc).

4.3. Molecular modelling studies

All the *in silico* investigations were performed on the High performance Graphics processing Unit installed with the Cent OS version 7. The hardware stipulations include the Intel core i7 processor of 8 cores and 16 GB RAM speed whereas the software stipulations include the commercial version of Schrödinger software package and the academic version of Desmond.

4.3.1. Protein and ligand preparation

The three dimensional crystal structure of the receptor protein Acetylcholinestarase (ACHE) containing the PDB ID: 4M0E has been obtained from Protein Data Bank (PDB). The crystal structure of the protein was not ready to be used in the theoretical calculations and hence, the target protein was prepared through the Protein Preparation Wizard implements in Maestro 11.3 [27] in which Prime loop modelling adds the missing residues. Initially, assignment of the bond orders, addition of hydrogen atoms and the removal of crystallographic water molecules were performed. Optimization of the hydroxyl group rotation, hydrogen-bonding network and thiol hydrogen will be performed with the protassign script which also generates the HIS protonation ann tautomerization states. This script also performs the chi flips in ASN, GLN and HIS residues. Minimization of the optimized structure of ACHE is performed with the help of OPLS-2005 force field till the root mean square deviation (RMSD) of the non-hydrogen atoms reaches 0.3 Å. The ligand molecule α-Bisabolol β-D-fucopyranoside was retrieved from PubChem in its 2-Dimensional structure and optimized into the 3-dimensonal structure using the LigPrep [28].

4.3.2. Molecular docking analysis

The Glide module implemented in Schrödinger possess the docking protocol and it was carried out in the current study [29]. This tool performs the grid-based ligand docking with searches accounting for the favorable interactions between one or more small molecule with the bimolecule, especially the protein. In this docking strategy, the ligand will be docked into the active site with the threshold of 0.50 kcla/mol for avoiding the minimized pose. The internal generation of conformations passing through the filters helps in the maintenance of the flexible ligand sampling. The receptor grid was generated with the predicted active site through sitemap. Ligand docking was utilized to carry out the docking of all ligands with the various charges. Initially, the ligand molecule was centered and subsequently they were allowed to rotate around three enagles. Secondly, the grid-based force field evaluation and the refinement of the docking including the torsional and rigid body movements of the ligands were supported out through the OPLS-AA force field. The glide score generation was carried out with the following formula.

$$\text{GScore} = a* \text{vdW} + b* \text{Coul} + \text{Lipo} + \text{Hbond} + \text{Metal} + \text{BuryP} + \text{RotB} + \text{Site}. \quad (1)$$

where, vdW = van der Waal energy, Coul = Coulomb energy, Lipo = lipophilic contact term, Hbond = hydrogen-bonding term, Metal = metal-binding term, BuryP = penalty for buried polar groups, RotB = penalty for freezing rotatable bonds, Site = polar interactions at the active site [30].

4.3.3. Binding free energy calculation

The free energy of the binding for the complexes obtained from the docking protocol were calculated using the Prime MM-GB/SA approach [31]. During this process, minimization of the docked poses with the local optimization feature and the complex energy were generated with the help of OPLS-AA (2005) force field and generalized Born/Surface area (GB/SA) continuum solvent model. The binding free energy of the complex were calculated with the following equations (2)–(5) [32a–d]

$$\Delta G_{bind} = \Delta E + \Delta G_{solv} + \Delta G_{SA} \quad (2)$$

$$\Delta E = E_{complex} - E_{receptor} - E_{ligand} \quad (3)$$

where, $E_{complex}$, $E_{receptor}$, and E_{ligand} are the minimized energies of the receptor-ligand complex, receptor and ligand, respectively. Prime uses the SGB model which employs the Gaussian surface instead of the van der Waals surface for the improved depiction of the solvent-accessible surface area.

$$\Delta G_{solv} = G_{solv}(\text{complex}) - G_{solv}(\text{receptor}) - G_{solv}(\text{ligand}) \quad (4)$$

where, G_{solv}(complex), G_{solv}(receptor), and G_{solv}(ligand) are the solvation free energies of the complex, receptor, and ligand, respectively.

$$\Delta G_{SA} = G_{SA}(\text{complex}) - G_{SA}(\text{receptor}) - G_{SA}(\text{ligand}) \quad (5)$$

where, G_{SA}(complex), G_{SA}(receptor), and G_{SA}(ligand) are the surface area energies for the complex, protein, and ligand, respectively. The reasonable criteria for the choice of best complexes based on scoring and interaction parameters were shown in XP docking with different charge model of ligands.

4.4. Determination of AChE activity

Acetylcholinesterase is the main pathological hallmark of AD. Briefly, AChE inhibitory activity was performed by previous reported method with slight modifications [33]. Different concentrations (10–50 μg/ml) of ABFP were incubated with 10 μl of AChE for 45 min at room temperature. After the incubation period, 125 μl of DTNB (3 mM) was added and the total volume was made up to 300 μl with 50 mM of Tris-HCl buffer (pH 8.0). Consequently, 50 μl of 15 mM Acetylthiocholine iodide was added to the reaction mixture to facilitate the initiation of the enzyme activity. Then, 3 mM 5-thio-2-nitrobenzoate was added to form the yellow color and inhibition of absorbance was read at the wavelength of 405 nm using UV–Visible spectrophotometer (U-2800, Hitachi, Japan). The experiments were performed in triplicates. Donepezil, was used as a standard drug and the percentage of inhibition was calculated according to the formula,

$$\textbf{Percentage of Inhibition} = \frac{\textbf{Sc} - \textbf{St X } 100}{\textbf{Sc}}$$

where S_c is the Specific activity of control group and S_t is the Specific activity of treated group.

4.5. In vitro antioxidant assays

4.5.1. Free radical scavenging assay

The antioxidant capacity of ABFP was estimated by method of Blois MS, 1958 [34]. 0.1 mM of DPPH (0.2 mL) mixed with 3 mL of methanol solution was added to various concentrations of ABFP (10–50 μg/ml). The change in the colour of the solution from purple to yellow was measured after 30 mins using UV–visible spectrophotometer (U-2800 model, Hitachi, Japan). Standard drug BHT (1 mg/ml) was used as a positive control and the percentage of inhibition was calculated according to the formula,

$$\%\ \textbf{DPPH scavenging activity} = \frac{(\textbf{Absc} - \textbf{Abst})}{(\textbf{Absc})}$$

where (Abs_c) is the Absorbance of control and (Abs_t) is the Absorbance of test.

4.5.2. Hydrogen peroxide scavenging assay

The hydrogen peroxide scavenging ability of ABFP was determined according to the method of Khan et al. [35]. Hydrogen peroxide solution (40 mM, pH 7.4) was added to various concentrations (10–50 μg/ml) of ABFP. The mixture was kept at room temperature for 10 min, after which the absorbance of Hydrogen peroxide was measured at 550 nm using phosphate buffer as blank. L- Ascorbic acid (1 mg/ml) was used as a positive control and the percentage of scavenging activity was calculated according to the formula,

$$\%(\mathbf{H2O2\ \ scavenging\ \ activity}) = \frac{(\mathbf{Absorbance\ \ of\ \ control}) - (\mathbf{Absorbance\ \ of\ \ test})}{(\mathbf{Absorbance\ \ of\ \ control})}$$

4.5.3. Hydroxyl radical scavenging activity

The Hydroxyl radical scavenging activity of ABFP was determined by using deoxyribose method as described in the literature [36]. The reaction mixture (1 mL) containing 1 mM ETDA, 10 mM $FeCl_3$, 10 mM deoxyribose, ABFP (10–50 μg/ml), 10 mM H_2O_2, 1 mM ascorbic acid and phosphate buffer (pH7.4) was incubated for 1 h at 37 °C. The reaction mixture was heated at 95 °C in a water bath for 20 mins, finally added 0.5 mL of 10% TCA and 0.5 mL of 0.4% TBA to form a pink colour. The absorbance of hydroxyl radical was measured at 532 nm. Butylated hydroxytoluene was used as the standard and the % of inhibition of hydroxyl radical was determined by comparison with control and test sample.

4.5.4. Total reducing power assay

The reducing potential of ABFP was evaluated according to the method of Moein et al. [37]. Different concentrations of the ABFP (10–50 μg/ml) was mixed with 0.5 mL of phosphate buffer solution (0.2 mM, pH 6.6), 1% of potassium ferrocyanide (0.5 mL) and incubated at 50 °C for 20 min. After the incubation period, 0.5 mL of 10% trichloro acetic acid was added and the mixture was centrifuged at 3000 rpm for 10 mins. The upper layer was collected, mixed with 0.5 mL of distilled water and 100 μl of 0.1% $FeCl_3$. The absorbance was measured at 700 nm. The higher absorbance of the sample indicates higher reducing power capacity. Ascorbic acid was used as the standard.

4.5.5. Metal chelating power assay

The metal chelating ability was carried out using the published method of Haro-Vicente et al [38]. In brief, the solution of Ferrous Sulphate (0.15 mM) was added to different concentrations of (10–50 μg/ml) of ABFP. The mixture of solution was reacted by the addition of 0.5 mM of Ferrozine and shaken robustly and incubated for 10 mins at room temperature. The absorbance of the solution was read at 562 nm. BHT was used as a positive control. The rate of inhibition of Fe^{2+}-ferrozoine complex formation was calculated as follows

$$\%\mathbf{of\ \ inhibition} = \frac{\mathbf{Absc - Abst}}{Absc} \times 100$$

where Abs c is the Absorbance of control and Abs t is the Absorbance of test.

4.5.6. Total antioxidant capacity assay

The total antioxidant potential of ABFP was evaluated by phosphomolybdenum method [23]. Briefly, different concentrations (10–50 μg/ml) of ABFP were mixed with 3 mL of reagent solution containing (0.6 M) H_2SO_4, (28 mM) NaH_2PO_4 and 4 mM $(NH_4)_2MoO_4$ and the reaction solution was incubated at 95 °C for 90 min. L-ascorbic acid was used as positive control and the absorbance was measured at 665 nm.

4.6. Preparation of $A\beta_{25–35}$ and analysis of antiaggregation and disaggregation property

$A\beta_{25–35}$ peptide (0.5 mg powder form) was dissolved in 500 μl of hexafluoro-2-propanol and kept in room temperature for 24 h to form monomers. Before start the experiments the dried powder was mixed with 500 μl sterile MilliQ water.

Phase I: Inhibition of formation of aggregates from oligomers: In phase I study, the monomeric $A\beta_{25–35}$ (100 μM) was incubated at 37 °C in 50 mM Tris-HCl buffer (pH 7.4) for 24 h to form oligomers. To this mixture of oligomers, ABFP (5 & 10 μg/ml) and Galantamine (50 μg/ml) was added and incubated for 24 & 48 h. After that, samples were taken for Thioflavin –T assay and Confocal microscopy study from the mixture of 24 & 48 h.

Phase II: Disaggregation of the pre-formed mature fibrils: In phase II study, $A\beta_{25–35}$ (100 μM) was incubated at 37 °C in 50 mM Tris-HCl buffer (pH 7.4) for 96 h to form mature fibrils. It was then treated with ABFP (5 & 10 μg/ml) and Galantamine (50 μg/ml) and incubated for 96 h and 9 days separately. For evaluation of the formation of pre -formed mature fibrils, samples from the mixture of 96 h and 9 days incubation were taken for Thioflavin –T assay and Confocal microscopy study (Fig. 5A).

4.6.1. Thioflavin T assay

Aβ fibrils were quantified by Thioflavin T assay [39]. Aliquots (5 μl) from the mixture of samples taken from both phases I & II solutions containing $A\beta_{25-35}$ with/without ABFP (24 h, 48 h, 96 h, 9 d) were added to 5 μM Thioflavin-T and final volume was made up to 300 μl of 50 mM glycine-NaOH buffer (pH 8.5). The fluorescence intensities were measured at wavelength of excitation 450 and emission 485 nm using spectrofluorimeter (Molecular Device SpectramaxM3, USA). The background ThT fluorescence was subtracted from the experimental values of all the samples. Galantamine (50 μM) was used as a positive control.

4.6.2. Fluorescence microscopic analysis

For the fluorescence microscopic study, 2.5 μl of the investigational samples (aliquots from 24 h, 48 h, 96 h, 9 d of Phase I and II experiments) were diluted with 5 μM of thioflavin T and incubated for 10 mins at RT, and then transferred onto a slide. $A\beta_{25–35}$ aggregation was visualized and captured by Confocal Laser Scanning Microscope FV300, Olympus, Japan.

4.7. Molecular dynamics simulation

The molecular dynamics simulation of the five copies of the Aβ peptides obtained from the PDB with the ID: 1QXC were randomly placed with the ABFP with the Desmond package [32d] with the Optimized Potentials for Liquid Simulations (OPLS) 2005 force field [40] for the minimization of the system. The peptide structure and the ligand were imported with the Monte Carlo simulated water model of TIP3-Pand solvated in an orthorhombic periodic box with the buffered space of 10 Å from the edges of the peptide so that it will not collide with the solvation box which is neutralized with the appropriate number of counter ions and 0.15 M salt concentration [41a–e]. The simulation system was comforted with the constant NPT (number of atoms N, pressure P and temperature, T) ensemble condition for the generation of the simulation data for the post simulation analyses. The steepest descent method helps in the energy minimization of the prepared system with the maximum of 5000 steps till the gradient threshold (25 kcal/mol/Å) is attained. Equilibration of the system has been achieved with the default protocol available in Desmond. The equilibrated system were carried forward in order to execute the molecular

dynamics simulation of 100 ns time period at the constant temperature and pressure of 300 K and 1 atm respectively with the time step of 2 fs.

4.8. Cell culture

The Neuro 2a cells were purchased from National Centre for Cell Sciences (NCCS), India. The cells were supplied with Dulbecco's modified Eagle medium (DMEM) supplemented with 5% CO_2, 10% horse serum, 15% Fetal bovine serum, 100 mg/ml streptomycin, 100 U/ml penicillin antibiotic and maintained at 37 °C.

4.9. Assessment of cell viability by MTT assay

The defensive dose was fixed by using the method of colorimetric MTT assay. Initially, the Neuro2a cells were plated at 2×10^5 cells/ml (per well) in a 96 well plate and incubated for 24 h for allowing the cells to adhere. Subsequently, Neuro2a cells were pre-treated with various concentrations of ABFP (2.5–10 µg/ml) for 24 h. Then, the cells were resuspended in 100 µl of MTT (0.5 mg/ml) and incubated for 4 h at 37 °C. Finally, the MTT was removed from the wells and washed with PBS and 100 µl of dimethylsulfoxide (DMSO) was added to each well. The absorbance was measured at 570 nm using multi well plate reader [42].

4.9.1. Neuroprotective effect of ABFP against $A\beta_{25\text{-}35}$ induced toxicity in Neuro2a cells

Based on our recent report that treatment of Neuro2a cells with 50 µM $A\beta_{25\text{-}35}$ caused an obvious decrease in the viability of the cells [25], the dosage of 50 µM of $A\beta_{25\text{-}35}$ was fixed for further assays. In this assay, the neuro2a cells (2×10^5 cells/ml) were grown in a 96 well plate and incubated for 24 h. After that the cells were pre-treated with the fixed concentration of ABFP (5 & 10 µg/ml) for 2 h, followed by treatment with 50 µM of $A\beta_{25\text{-}35}$ for 24 h. Subsequently, MTT solution was added to all the wells and incubated at 37 °C for 4 h. After that, the MTT solutions were removed and washed with PBS. Finally, 300 µl of DMSO was added and the absorbance was measured at 570 nm. Results were expressed as percentage of viability and compared with control samples [43]. In addition, the morphological characteristics of cells were observed in the phase contrast microscope analysis.

$$\textbf{Cell viability } (\%) = \frac{\textbf{Absorbance in test well}}{\textbf{Absorbance in control well}} \times 100$$

4.10. Measurement of intracellular reactive oxygen species (ROS) level

The measurement of intracellular ROS was assessed using ROS-sensitive 2′,7′-dichlorodihydrofluorescein diacetate staining method [26]. In this assay, Neuro2a cells (2×10^5 cells/ml) were pre-treated with ABFP (5 & 10 µg/ml) and then exposed to 50 µM of $A\beta_{25\text{-}35}$ for 24 h. Following treatments, the medium was discarded and incubated with 10 µM of DCFH-DA for 20 min at RT. After that, phosphate buffer solution (pH 7.4) was used to wash the cells and lysed with lysis buffer (pH 8.0). Finally, the fluorescence intensity was measured at an excitation wavelength of 495 nm and an emission wavelength of 520 nm by using SpectraMax M3 Microplate Reader. The amount of ROS produced was determined from the fluorescent intensity observed in the samples.

4.11. Statistical analysis

All the experiments were done in triplicates and the statistical analysis was performed by one-way ANOVA using SPSS 17 statistical software followed by Duncan's test. $P < 0.05$ was considered as statistically different between control and treated groups.

Acknowledgements

The authors MJ, SS and KPD wish to acknowledge the Computational and Bioinformatics Facility provided by the Alagappa University Bioinformatics Infrastructure Facility (funded by DBT, India; GOI; File No. BT/BI/25/012/2012, BIF), DST-FIST, India (Grant No. SR/FST/LSI-639/2015(C)) and UGC-SAP, India (Grant No. F.5-1/2018/DRS-II (SAP-II)). The authors SV and SKS acknowledge the financial support of DST-FIST [SR/FST/LSI-667/2016(C)]. All the authors of Alagappa University acknowledge the financial support of DST-PURSE, India (Grant No. SR/PURSE Phase 2/38 (G)) and MHRD-RUSA 2.0 [F. 24-51/2014-U, Policy (TN Multi-Gen), Dept of Edn, GoI] for providing the infrastructure facilities and the University Science Instrumentation Centre (USIC), Alagappa University, Karaikudi, Tamil Nadu, India for providing the Instrumentation facility.

Appendix A. Supplementary material

Supplementary data to this article can be found online at https://doi.org/10.1016/j.bioorg.2019.102935.

References

[1] C. Zhang, Q.Y. Du, L.D. Chen, W.H. Wu, S.Y. Liao, L.H. Yu, X.T. Liang, Design, synthesis and evaluation of novel tacrine-multialkoxybenzene hybrids as multi-targeted compounds against Alzheimer's disease, Eur J Med Chem. 116 (2016) 200–209.
[2] A. Alzheimer's, Alzheimer's disease facts and figures, Alzheimers Dement 11 (2015) 332.
[3] Y. Li, X. Qiang, L. Luo, Y. Li, G. Xiao, Z. Tan, Y. Deng, Synthesis and evaluation of 4-hydroxyl aurone derivatives as multifunctional agents for the treatment of Alzheimer's disease, Bioorgan Med Chem. 24 (2016) 2342–2351.
[4] N. Guzior, M. Bajda, J. Rakoczy, B. Brus, S. Gobec, B. Malawska, Isoindoline-1, 3-dione derivatives targeting cholinesterases: Design, synthesis and biological evaluation of potential anti-Alzheimer's agents, Bioorgan. Med. Chem. 23 (2015) 1629–1637.
[5] J.B. Shaik, B.K. Palaka, M. Penumala, K.V. Kotapati, Kotapati, S.R. Devineni, S. Eadlapalli, G.D. Amooru, Synthesis pharmacological assessment, molecular modeling and in silico studies of fused tricyclic coumarin derivatives as a new family of multifunctional anti-Alzheimer agents, Eur. J. Med. Chem. 107 (2016) 219–232.
[6] P. Meena, V. Nemaysh, M. Khatri, A.P.M. Luthra, M. Tiwari, Synthesis, biological evaluation and molecular docking study of novel piperidine and piperazine derivatives as multi-targeted agents to treat Alzheimer's disease, Bioorg. Med. Chem. Lett. 23 (2015) 1135–1148.
[7] M. Digiacomo, Z. Chen, S. Wang, A. Lapucci, M. Macchia, X. Yang, S. Rapposelli, Synthesis and pharmacological evaluation of multifunctional tacrine derivatives against several disease pathways of AD, Bioorg. Med. Chem. Lett. 25 (2015) 807–810.
[8] B. Shanmuganathan, D.S. Malar, S. Sathya, K.P. Devi, Antiaggregation potential of Padina gymnospora against the toxic Alzheimer's β-amyloid peptide25–35 and cholinesterase inhibitory property of its bioactive compounds, PloS One 10 (2015).
[9] V. Kren, L. Martínková, Glycosides in medicine: "The role of glycosidic residue in biological activity, Curr. Med. Chem. 8 (2001) 1303–1328.
[10] M. Piochon, J. Legault, C. Gauthier, A. Pichette, Synthesis and cytotoxicityevaluation of natural α-bisabolol β-D-fucopyranoside and analogues, Phytochem. 70 (2009) 228–236.
[11] R.D. Egleton, S.A. Mitchell, J.D. Huber, M.M. Palian, R. Polt, T.P. Davis, Improved blood-brain barrier penetration and enhanced analgesia of an opioid peptide by glycosylation, J. Pharmacol. Exp. Ther. 299 (2001) 967–972.
[12] B. Mikhova, H. Duddeck, R. Taskova, M. Mitova, K. Alipieva, Oxygenated bisabolane fucosides from Carthamus lanatus L, Z. Naturforsch C. 59 (2004) 244–248.
[13] R.R. Schmidt, W. Kinzy, Anomeric-oxygen activation for glycoside synthesis: the trichloroacetimidate method, Adv. Carbohyd. Chem. Bi. 50 (1994) 21–123.
[14] A.J. Ross, I.A. Ivanova, M.A. Ferguson, A.V. Nikolaev, Parasite glycoconjugates. Part 11. 1, Preparation of phosphodisaccharide synthetic probes, substrate analogues for the elongating α-D-mannopyranosylphosphate transferase in the Leishmania, J. Chem. Soc. Perkin Trans. 1 (2001) 72–81.
[15] A. Pugazhendhi, R.B. Shafreen, K.P. Devi, N. Suganthy, Assessment of antioxidant, anticholinesterase and antiamyloidogenic effect of Terminalia chebula, Terminalia arjuna and its bioactive constituent 7-Methyl gallic acid–An in vitro and in silico studies, J. Mol. Liq. 257 (2018) 69–81.
[16] G. Brunhofer, A. Fallarero, D. Karlsson, A. Batista-Gonzalez, P. Shinde, C.G. Mohan, P. Vuorela, Exploration of natural compounds as sources of new bifunctional scaffolds targeting cholinesterases and beta amyloid aggregation: the case of chelerythrine, Bioorgan. Med. Chem. 2 (2012) 6669–6679.
[17] D.A. Butterfield, C.M. Lauderback, Lipid peroxidation and protein oxidation in Alzheimer's disease brain: Potential causes and consequences involving amyloid β-peptide-associated free radical oxidative stress1, 2, Free Radical Bio. Med. 32

(2002) 1050–1060.
[18] I. Gulcin, M. Emin, M.E. Buyukokuroglu, O.I. Kufrevioglu, Metal chelating and hydrogen peroxide scavenging effects of melatonin, J. Pineal Res. 34 (2003) 278–281.
[19] M.H. Gordon, The mechanism of antioxidant action in vitro, In Food antioxidants, 1990, pp. 1–18.
[20] S. Meir, J. Kanner, B. Akiri, Determination and involvement of aqueous reducing compounds in oxidative defense systems of various senescing leaves, J. Agric. Food Chem. 43 (1995) 1813–1815.
[21] C.S. Atwood, X. Huang, R.D. Moir, R.E. Tanzi, A.I. Bush, Role of free radicals and metal ions in the pathogenesis of Alzheimer's disease, Met. Ions Biol. Syst. 36 (1999) 309–364.
[22] N.G. Faux, C.W. Ritchie, A. Gunn, A. Rembach, A. Tsatsanis, J. Bedo, PBT2 rapidly improves cognition in Alzheimer's disease: additional phase II analyses, J. Alzheimers Dis. 20 (2010) 509–516.
[23] P. Prieto, M. Pineda, M. Aguilar, Spectrophotometric quantitation of antioxidant capacity through the formation of a phosphomolybdenum complex: specific application to the determination of vitamin E, Anal. Biochem. 269 (1999) 337–341.
[24] N. Suganthy, V.S. Ramkumar, A. Pugazhendhi, G. Benelli, G. Archunan, Biogenic synthesis of gold nanoparticles from Terminalia arjuna bark extract: assessment of safety aspects and neuroprotective potential via antioxidant, anticholinesterase, and antiamyloidogenic effects, Environ. Sci. Pollut. R 1–16 (2017).
[25] S. Sathya, B. Shanmuganathan, G. Manirathinam, K. Ruckmani, K.P. Devi, α-Bisabolol loaded solid lipid nanoparticles attenuates Aβ aggregation and protects Neuro-2a cells from Aβ induced neurotoxicity, J. Mol. Liq. 264 (2018) 431–441.
[26] B. Muthaiyah, M.M. Essa, V. Chauhan, A. Chauhan, Protective effects of walnut extract against amyloid beta peptide-induced cell death and oxidative stress in PC12 cells, Neurochem Res. 36 (2011) 2096–2103.
[27] Protein Preparation Wizard, Schrödinger, NY, 2017.
[28] Ligprep, Schrodinger, NY, 2017.
[29] Glide, Schrodinger, NY, 2017.
[30] R.A. Friesner, R.B. Murphy, M.P. Repasky, L.L. Frye, J.R. Greenwood, T.A. Halgren, P.C. Sanschagrin, D.T. Mainz, Extra precision glide: docking and scoring incorporating a model of hydrophobic enclosure for protein-ligand complexes, J. Med. Chem. 49 (2006) 6177–6196.
[31] Prime, Schrodinger, NY, 2017.
[32] (a) J. Li, R. Abel, K. Zhu, Y. Cao, S. Zhao, R.A. Friesner, The VSGB 2.0 model: a next generation energy model for high resolution protein structure modeling, Proteins 79 (2011) 2794;
(b) P.D. Lyne, M.L. Lamb, J.C. Saeh, Accurate prediction of the relative potencies of members of a series of kinase inhibitors using molecular docking and MM-GBSA scoring, J. Med. Chem. 16 (2006) 4805–4808;
(c) S.K. Tripathi, S.K. Singh, Insights into the structural basis of 3,5-diaminoindazoles as CDK2 inhibitors: prediction of binding modes and potency by QM-MM interaction, MESP and MD simulation, Mol. Biosyst. 10 (2014) 2189–2201;
(d) K.K. Reddy, S.K. Singh, Combined ligand and structure-based approaches on HIV-1 integrase strand transfer inhibitors, Chem.-Biol. Interact. 218 (2014) 71–81.
[33] G.L. Ellman, K.D. Courtney, V. Andres Jr, R.M. Featherstone, A new and rapid colorimetric determination of acetylcholinesterase activity, Biochem. Pharmacol. 7 (1961) 88–95.
[34] M.S. Blois, Antioxidant determinations by the use of a stable free radical, Nature 181 (1958) 1199.
[35] R.A. Khan, M.R. Khan, S. Sahreen, M. Ahmed, Evaluation of phenolic contents and antioxidant activity of various solvent extracts of Sonchus asper (L.) Hill, Chem. Cent. J. 6 (2012) 12.
[36] B. Lipinski, Hydroxyl radical and its scavengers in health and disease, Oxid. Med. Cell Longev. 7 (2011) 9.
[37] M.R. Moein, S. Moein, S. Ahmadizadeh, Radical scavenging and reducing power of Salvia mirzayanii subfractions, Molecules 13 (2008) 2804–2813.
[38] J.F. Haro-Vicente, C. Martinez-Gracia, G. Ros, Optimization of in vitro measurement of available iron from different fortificants in citric fruit juices, Food Chem. 98 (2006) 639–648.
[39] S.A. Hudson, H. Ecroyd, T.W. Kee, J.A. Carver, The thioflavin T fluorescence assay for amyloid fibril detection can be biased by the presence of exogenous compounds, FEBS 276 (2009) 5960–5972.
[40] Desmond, Schrodinger, NY, 2017.
[41] (a) S. Sirin, D.A. Pearlman, W. Sherman, Physics-based enzyme design: predicting binding affinity and catalytic activity, Proteins 82 (2014) 3397–3409;
(b) W.L. Jorgensen, J. Chandrasekhar, J.D. Madura, R.W. Impey, M.L. Klein, Comparison of simple potential functions for simulating liquid water, J. Chem. Phys. 79 (1983) 926–935;
(c) P. Mark, L. Nilsson, Structure and dynamics of the TIP3P, SPC, and SPC/E water models at 298 K, J. Phys. Chem. A 105 (2001);
(d) Z.U. Guo, U.J. Mohanty, J.T.K. Noehre, T.K.W. Sawyer, W.G. Sherman, G. Krilov, Probing the α-helical structural stability of stapled p53 peptides: Molecular dynamics simulations and analysis, Research article Chem. Biol. Drug Des. 75 (2010) 348–359;
(e) V. Suryanarayanan, S.K. Singh, Assessment of dual inhibition property of newly discovered inhibitors against PCAF and GCN5 through in silico screening, molecular dynamics simulation and DFT approach, J. Recept Sig. Transd. 18 (2014) 1–11.
[42] B. Shanmuganathan, V. Suryanarayanan, S. Sathya, M. Narenkumar, S.K. Singh, K. Ruckmani, K.P. Devi, Anti-amyloidogenic and anti-apoptotic effect of α-bisabolol against Aβ induced neurotoxicity in PC12 cells, Eur. J. Med. Chem. 143 (2018) 1196–1207.
[43] S. Sathya, B. Shanmuganathan, S. Saranya, S. Vaidevi, K. Ruckmani, K. Pandima Devi, Phytol-loaded PLGA nanoparticle as a modulator of Alzheimer's toxic Aβ peptide aggregation and fibrillation associated with impaired neuronal cell function, Artif. Cell. Nanomed. B (2017) 1–12.